JOURNAL OF GEOPHYSICAL RESEARCH, VOL. 95, NO. C9, PAGES 16,055–16,063, SEPTEMBER 15, 1990

Model-Data Comparisons of Moments of Nonbreaking Shoaling Surface Gravity Waves

STEVE ELGAR

Electrical and Computer Engineering, Washington State University, Pullman

M. H. FREILICH

Jet Propulsion Laboratory, California Institute of Technology, Pasadena

R. T. GUZA

Center for Coastal Studies, Scripps Institution of Oceanography, La Jolla, California

The predictions of linear and nonlinear (Boussinesq) shoaling wave models for nonbreaking unidirectional surface gravity waves are compared to field observations, with particular emphasis on quantities that may be important for cross-shore sediment transport. The extensive data sets were obtained on two natural beaches, span water depths between 1 and 10 m, and include incident wave power spectra with narrow, broad, and bimodal shapes. Significant wave heights varied between approximately 30 and 100 cm, and peak periods between approximately 8 and 18 s. The evolution of total variances of sea surface elevation, cross-shore velocity, and horizontal acceleration is modeled at least qualitatively well by both linear and nonlinear theories. Only the nonlinear theory predicts the increasingly asymmetric sea surface elevations and horizontal velocities (pitched-forward wave shapes) and the weaker variation of skewness (difference between crest and trough profiles) which are observed to occur during shoaling. The nonlinear theory also models qualitatively well the large skewed accelerations which occur during the passage of asymmetric waves.

1. INTRODUCTION

Much theoretical, numerical, laboratory, and field work has described the evolution of ocean surface gravity waves propagating through the shoaling region and surf zone. The wave hydrodynamics are of interest, but the studies have also been motivated by recognition of the close coupling between wave-induced fluid motions and sediment transport. The present work compares extensive observations of nonbreaking waves on two natural beaches with predictions of shoaling wave models, with emphasis on quantities that may be important for predicting cross-shore sediment transport.

Both linear and nonlinear theories have been used to model shoaling waves. Models based on linear, finite depth theory (LFDT) [*Collins*, 1972; *Lé Mehauté and Webb*, 1982] can be used to make relatively accurate predictions of integrated second-order moments (e.g., total variances) of sea surface elevations and horizontal velocities seaward of the breaking region. Although not as accurately, LFDT also predicts changes in the power spectra of elevations and currents before breaking occurs. With the inclusion of heuristic terms to model energy losses resulting from wave breaking, LFDT has been used to relate on-offshore changes in wave heights on natural beaches to offshore wave conditions, on-offshore propagation distance, and depth [*Battjes and Janssen*, 1978; *Guza and Thornton*, 1980, 1985; *Thornton and Guza*, 1983; *Dally et al.*, 1985].

However, many modern sediment transport models [e.g., *Bjiker et al.*, 1976; *Bowen*, 1980; *Bailard and Inman*, 1981] relate net sediment transport to small deviations from symmetry in the on-offshore velocity field. In addition, recent data suggest that suspended sediment concentrations are correlated with near-bottom horizontal accelerations [*Hanes and Huntley*, 1986], and thus skewness in the acceleration field may also be related to net sediment transport. *Elgar et al.* [1988] showed that immediately seaward of the break zone the horizontal velocity field was highly asymmetric (differences between front and rear face profiles) and only moderately skewed (differences between crest and trough profiles), while the acceleration field had high values of both skewness and asymmetry. The commonly used second-order statistics contain no information on wave shapes and hence cannot be used as input to on-offshore sediment transport models that are sensitive to velocity or acceleration skewness and asymmetry.

Skewness, asymmetry, and other third (and higher-order) odd moments that may play a role in net sediment transport are inherently nonlinear properties, and thus LFDT cannot predict their evolution through the shoaling region. Recently, nonlinear shoaling models based on the Boussinesq equations [*Peregrine*, 1967, 1972, 1983] have been shown to predict accurately many features of nonbreaking waves in shallow water. In general, the Boussinesq equations include the effects of shoaling, refraction, reflection, and diffraction for weakly nonlinear, weakly dispersive arbitrary wave fields (i.e., directionally spread and broad banded in frequency), although most implementations of Boussinesq shoaling models include only a subset of these phenomena. Boussinesq-based wave evolution models have been tested successfully against a variety of laboratory data, including

Paper number 90JC00963.
0148-0227/90/90JC-00963$05.00

monochromatic, unidirectional shoaling waves [*Abbott et al.*, 1978; *Madsen and Warren*, 1984], monochromatic, directional waves refracting over a topographical lens [*Liu et al.*, 1985; *Madsen and Warren*, 1984; *Rygg et al.*, 1988], monochromatic, directional waves propagating through a harbor [*Abbott et al.*, 1978], and monochromatic waves reflecting from and transmitting through a porous breakwater [*Abbott et al.*, 1978; *Madsen and Warren*, 1984]. Dissipation owing to bottom drag was heuristically incorporated in the Boussinesq model of *Madsen and Warren* [1984]. Boussinesq models also compare favorably to various analytical nonlinear solutions, including refracting cnoidal waves [*Madsen and Warren*, 1984; *Liu et al.*, 1985; *Rygg et al.*, 1988], cnoidal waves diffracting along a breakwater [*Yoon and Liu*, 1989*a*], and cnoidal waves interacting with a current [*Yoon and Liu*, 1989*b*]. *Boczar-Karakiewicz and Davidson-Arnott* [1987] combined a unidirectional, monochromatic Boussinesq wave model with a sediment transport model sensitive to velocity skewness and qualitatively predicted sandbar wavelengths in Georgian Bay, Lake Huron (see also *Elgar et al.* [1990]).

By comparing many field data sets (acquired on two separate beaches and spanning a range of incident wave conditions) with model predictions, the present study evaluates the accuracy of a one-dimensional Boussinesq shoaling model [*Freilich and Guza*, 1984] for prediction of second and third moments of the horizontal velocity and acceleration fields. In addition, extensive new model-data comparisons of sea surface elevation statistics in 4–10 m depth are presented, expanding on the limited subset of data analyzed by *Freilich and Guza* [1984]. The model performance is good. Statistics of the spatial evolution of sea surface elevation, velocity, and acceleration are predicted well for a wide range of ocean conditions, and wave fields with similar initial spectral shapes evolve similarly on the two separate beaches considered.

The nonlinear Boussinesq model is reviewed in section 2, and the field experiments and data reduction are briefly described in section 3. Comparisons of model predictions with field observations are presented in section 4. Conclusions follow in section 5.

2. BOUSSINESQ MODEL

Freilich and Guza [1984] and *Liu et al.* [1985] respectively have derived one- and two-dimensional nonlinear shoaling models based on perturbation solutions to the Boussinesq equations. The models clearly identify nonlinear near-resonant triad interactions as the primary cause for evolution of third moments of the wave field. The one-dimensional, many-mode (i.e., broad banded in frequency) Boussinesq model has been compared to a limited set of ocean field data [*Freilich and Guza*, 1984; *Elgar and Guza*, 1985*a*, 1986].

The Boussinesq equations require both shallow water depths ($(kh)^2 \ll 1$, where k is the wave number and h is the water depth) and small wave amplitudes ($a/h \ll 1$, where a is the wave amplitude) such that the Ursell number, $U = (a/h)/(kh)^2$ is approximately unity. The one-dimensional shoaling model assumes that the waves are normally incident to a beach with plane-parallel contours, and it neglects dissipation and reflection.

The model is cast in terms of coupled, nonlinear, ordinary differential equations with the (temporal) Fourier coefficients of the wave field as the dependent variables. Since the model describes the spatial evolution of the Fourier coefficients (i.e., both the amplitudes and phases), it contains information relating to wave shapes and instantaneous oscillatory velocities.

Freilich and Guza [1984] give details of implementing the nonlinear model. Fourier coefficients used as initial conditions for nonlinear model predictions are provided by measurements at the seaward edge of the region of interest. The model equations are then integrated numerically, yielding predicted values of Fourier coefficients of sea surface elevation in shallower water. The predicted and observed Fourier coefficients can then be manipulated and compared in various ways. Alternatively, after inverse Fourier transforming the predicted coefficients, comparisons can be made between predicted and observed time series.

3. FIELD EXPERIMENTS AND DATA REDUCTION

Two field experiments conducted in 1980 (Torrey Pines and Santa Barbara, California) provide the data used for model verification. The bottom contours were relatively straight and parallel at both experimental sites, and the mean beach slopes through the shoaling region were 0.022 and 0.050 at Torrey Pines and Santa Barbara, respectively. Data were obtained from wave staffs and near-bottom pressure and electromagnetic current meters. The field experiments, including representative beach profiles and descriptions of the sensors and data reduction, are presented by *Freilich and Guza* [1984], *Elgar and Guza* [1985*a*, 1986], and *Thornton and Guza* [1986]. Measurements from cross-shore arrays extending for approximately 267 m (Torrey Pines) and 56 m (Santa Barbara) are used in the model-data comparisons presented below.

Initial conditions for the nonlinear Boussinesq shoaling model were generated with data from a bottom-mounted pressure sensor in 10 m depth at Torrey Pines and in 4 m depth at Santa Barbara. Short sections of data were Fourier transformed and converted to Fourier coefficients of sea surface elevation using linear finite depth theory. Results of integrations of the Boussinesq shoaling model for consecutive short sections were averaged together for statistical comparisons. The maximum frequencies considered were 0.234 and 0.4 Hz at Torrey Pines and Santa Barbara, respectively. The different cutoff frequencies reflect the requirement that the waves be relatively long compared to the depth, and the relatively deeper water at Torrey Pines.

All pressure and current meters were positioned within 80 cm of the seabed, and the pressure data were converted to sea surface elevation using linear theory. Because linear theory accurately relates local values of pressure and elevation in nonbreaking waves [*Guza and Thornton*, 1980, and references therein], hereinafter no differentiation will be made between direct measurements of sea surface elevation and sea surface elevation inferred from pressure data. Comparisons between model predictions and current meter data were made at the known depth of the current meter sensing element (i.e., no theory is applied to the current meter data).

Energy dissipation was not important in the model-data comparisons discussed here because the evolution distances were relatively short, white-capping was not pronounced, and the comparisons were terminated when measured energy losses owing to wave breaking were significant. The

Torrey Pines experiment was designed to study nonbreaking waves, and thus all sensors were seaward of the breaking zone and dissipation was found to be negligible. Many of the Santa Barbara sensors were sometimes within the surf zone, and the estimated dissipation was sometimes significant for the shallowest sensors (1.6–1.0 m depth). Model-data comparisons are presented only for sensors where the total shoreward energy flux (integrated over all frequencies) was at least 85% of the value measured at the most seaward instrument.

The effects of directional spread and/or nonnormal incidence in the incoming wave field on the nonlinear evolution of shoaling waves are not yet well understood. Boussinesq models appropriate for this case [e.g., *Liu et al.*, 1985] have not been applied to random ocean waves. The data sets discussed here include locally generated wind-driven seas having broad directional spread, as well as wave fields composed of swell and sea simultaneously arriving from different directional quadrants. Although the incident wave fields were neither unidirectional nor normally incident, accurate one-dimensional Boussinesq model predictions are possible because fundamentally nondirectional statistics are considered here. Moreover, as refracting surface waves propagate into shallower water, they are strongly polarized in the cross-shore direction, and thus the approximation of normal incidence often is not grossly violated. A longshore array of sensors in 10 m depth at Torrey Pines and a colocated pressure sensor-bidirectional current meter pair in 4 m depth at Santa Barbara showed that the principal wave directions at the offshore, initial conditions for the model predictions are less than 20° relative to normal incidence [*Freilich and Guza*, 1984; *Elgar and Guza*, 1985*a*; *Thornton and Guza*, 1986; *Freilich et al.*, 1990].

TABLE 1. Parameters for the Torrey Pines (S) and Santa Barbara (J, F) Data Sets

Data Set	H_{sig}, cm	T_p, s	Length, s	Depth, m
S3(1)	44	13, 8	9,216	10.0
S3(2)	48	13, 8	13,312	10.5
S3(3)	49	13, 8	19,456	10.3
S4	39	20, 13, 8	15,360	10.0
S8	53	13	26,624	10.1
S9	65	11	14,408	10.3
S10	68	16	20,480	10.1
S11	90	16	15,360	10.4
S12	72	14	13,312	10.3
S16	56	13, 5	15,360	10.3
S23	47	10	8,192	9.5
S24	56	10	5,120	10.9
J30	34	12, 7	9,216	4.1
F2	63	16	16,896	3.9
F3	96	15	8,192	3.9
F4	92	14	9,728	3.8
F12	57	18, 5	6,656	3.4
F15	66	15 (broad)	8,192	3.5

Data set names indicate the date of the data run (S is September, J is January, and F is February 1980). H_{sig} is the significant wave height (4 times the standard deviation of the sea surface) at the initial conditions. T_p is the period of the power spectral peak (periods from multipeaked spectra are in descending order of spectral level). Length is the duration of the data set. Depth is the water depth at the initial conditions.

4. MODEL-DATA COMPARISONS

Twelve data sets acquired at Torrey Pines and six from Santa Barbara are analyzed in this study. The significant wave height and peak period at the initial conditions and the length of each data set are given in Table 1. Using a representative subset of the data collected at Torrey Pines, *Freilich and Guza* [1984] found good agreement between model predictions of sea surface elevation and field observations at frequencies less than 0.234 Hz for depths between 10 and 4 m. *Elgar and Guza* [1985*a*, 1986] discussed the same Santa Barbara data sets considered here but primarily concentrated on bottom pressure and sea surface elevation and only briefly considered velocity. They found good agreement between model and data in depths between 4 and 1 m, for frequencies below 0.4 Hz. In very shallow water, immediately prior to wave breaking, a/h was as high as 0.25, and the model overpredicted the amplitudes of high-frequency components.

Each data set can be assigned to one of three qualitative categories based on the shape of the initial power spectrum: (1) narrow-band wave fields dominated by remotely generated swell, (2) broadband wave fields with significant variance at a variety of frequencies, and (3) bimodal wave fields with concentrations of energy at frequencies corresponding to both swell and locally generated sea. Measured wave fields within the same category evolved similarly, although details of the shoaling transformation can be sensitive to such variables as initial variance and phase coupling. Below, Boussinesq model predictions of second and third moments are compared in detail with observations of wave fields selected from each of the three categories. Following these detailed comparisons, observed and predicted statistics for all 18 data sets are presented.

4.1. *Narrow-Band Wave Fields*

Power spectra of sea surface elevation characteristic of frequency-sorted swell from a distant storm are shown in Figure 1 (S11 and F2, described in the caption). The observed evolution of second moments (i.e., variances) of sea surface elevation and near-bottom horizontal velocity and acceleration is predicted well by both linear theory and the nonlinear Boussinesq model (Figure 2).

In addition to the increase in variance during shoaling, the wave profiles evolve from nearly sinusoidal shapes in deeper water to positively skewed (sharp peaks and broad troughs) shapes to vertically asymmetric, sawtooth-type shapes just prior to breaking. The change in waveform during shoaling is statistically described by the evolution of third moments, skewness S and asymmetry A, which measure deviations from symmetry about horizontal and vertical axes, respectively [*Masuda and Kuo*, 1981; *Elgar and Guza*, 1985*b*]. A sawtooth shape (steep front faces and gently sloping rear faces, but crests and troughs of equal amplitudes) has $S = 0$ and $A \neq 0$, while a "Stokes wave" shape (broad, low troughs and narrow, tall crests but symmetric front and back faces) has $S \neq 0$ and $A = 0$. The sawtooth time series in Figure 3 and its Hilbert transform with Stokes-like shape illustrate the relationship between skewness, asymmetry, and wave shape [*Elgar*, 1987]. The difference between these two time series is the phase relationship between the primary frequency and the phase-locked harmonics; they have identical power spectra.

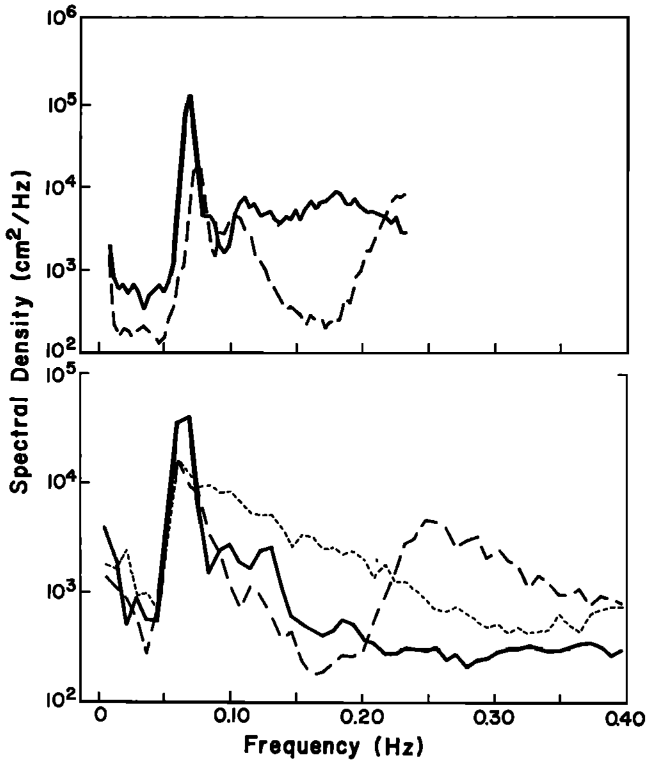

Fig. 1. Initial power spectra of sea surface elevation for the model predictions. (Top) Torrey Pines, $h \sim 10$ m (solid line, S11; dashed line, S16). (Bottom) Santa Barbara, $h \sim 4$ m (solid line, F2; dashed line, F12; dotted line, F15).

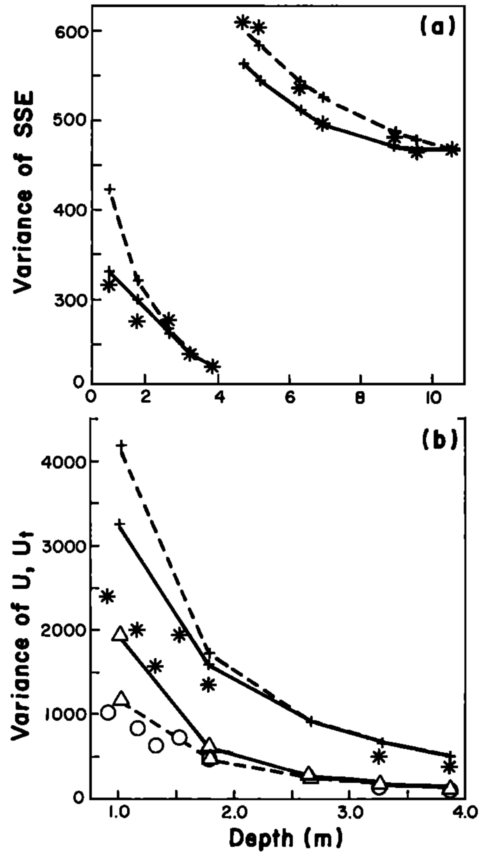

Fig. 2. Predicted and observed second moments versus depth for the narrow-band swell data ($h > 4$ m, Torrey Pines (S11); $h \leq 4$ m, Santa Barbara (F2)): (*a*) sea surface elevation (cm^2) and (*b*) near-bottom horizontal velocity (U; (cm/s)^2) and near-bottom horizontal acceleration (U_t; (cm/s^2)^2). Asterisks are observed values of sea surface elevation (Figure 2*a*) and velocity (Figure 2*b*) variance, and circles in Figure 2*b* are observations of acceleration variance. The solid (Boussinesq model) and dashed (LFDT model) lines are drawn through predictions (pluses and triangles) of the respective observed quantities. The slight discrepancies between observed and "predicted" values at the Santa Barbara initial conditions ($h \sim 4$ m, Figure 2*b*) are caused by differences between velocity inferred from pressure measurements ("predicted") and velocity measured directly with a current meter [*Guza and Thornton*, 1980]. For Figures 2, 4, and 6–12 the data have been band pass filtered between 0.04 and 0.234 Hz (Torrey Pines) and between 0.04 and 0.3 Hz (Santa Barbara).

The observed evolution of skewness and asymmetry for swell-dominated wave fields is displayed in Figure 4. Third moments are small in deep water ($A = S = 0$ for linear waves) and increase owing to nonlinear interactions during shoaling. In both the observations and the model predictions, skewness of sea surface elevation and velocity attains a maximum and then begins to decrease before the waves break. Asymmetry increases approximately monotonically, consistent with the increasingly steep, pitched-forward shape of shoaling waves. Since the model predictions of third moments in 4.5 m depth given 10 m depth initial conditions at Torrey Pines are very close to observed values at the Santa Barbara initial conditions (depth of 4 m, Figure 4), the necessary reinitialization of the model with field measurements at Santa Barbara does not appreciably detract from the nonlinear model's ability to predict sea surface elevation and near-bottom horizontal velocity moments up to the region of wave breaking ($\sim$1 m depth) given wave conditions in 10 m depth.

Although linear finite depth theory fairly accurately predicts the observed evolution of variances (Figure 2), LFDT cannot predict the changes in wave shape as the wave field shoals. Linear theory predicts $A = S = 0$ everywhere if the random phase assumption is invoked, and it predicts nearly constant A and S if the LFDT propagation model is initialized with skewed and/or asymmetric field measurements.

The changing wave profiles during shoaling can be seen in the time series shown in Figure 5. In 10 m depth (Figure 5*a*) the waves are nearly sinusoidal, but as they propagate into shallower water, their profiles become skewed and asymmetric (4.5 m depth, Figure 5*b*) and finally very asymmetric (1.5 m depth, Figure 5*d*). The change in wave profile is accurately predicted by the Boussinesq model (Figure 5). The asymmetric profiles near the breaking region (Figure 5*d*) result in strongly skewed horizontal accelerations, which are also accurately predicted by the Boussinesq model (Figure 5*e*).

Just as the power spectrum describes the frequency distribution of variance, the distribution of skewness and asymmetry as a function of frequency triads is described by the real and imaginary part of the bispectrum, respectively [*Hasselman et al.*, 1963; *Elgar and Guza*, 1985*b*). The ratio of imaginary to real parts of the bispectrum (the arc tangent of which is the biphase) is related to the wave profile. Stokes-type shapes have biphase of 0, while a sawtooth has biphase of $-\pi/2$. For wave fields dominated by narrow-band swell, nonlinear interactions between waves at the power spectral primary peak frequency f_p ($f_p = 0.06$ Hz for the

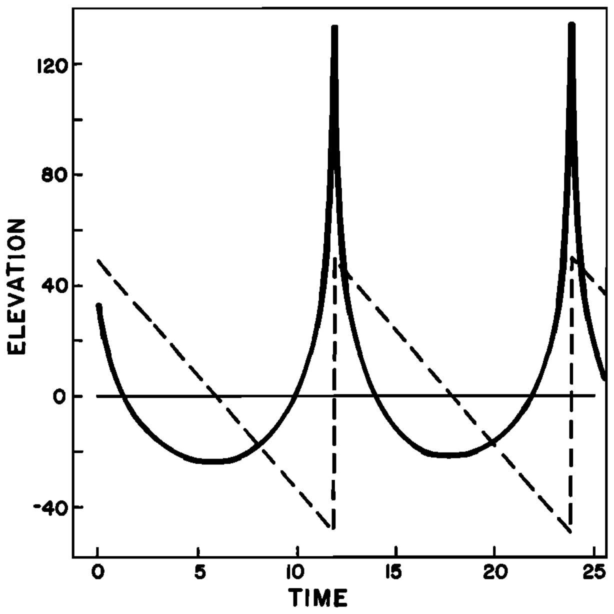

Fig. 3. Elevation versus time (units are arbitrary) of a sawtooth wave shape (dashed line, $S = 0$, $A = 2.3$) and its Hilbert transform (solid line, $S = 2.3$, $A = 0$).

narrow-band data discussed here) and those at the first few harmonics ($f_{2p}, f_{3p}, \cdots$) account for a large fraction of the total third moments [*Elgar and Guza*, 1985*b*; *Doering and Bowen*, 1987]. As shown in Figure 6 for sea surface elevation, the biphases of the self-self interaction (f_p, f_p, f_{2p}) and of the triad consisting of (f_p, f_{2p}, f_{3p}) evolve from near 0° in 10 m depth toward −90° as the depth decreases. The

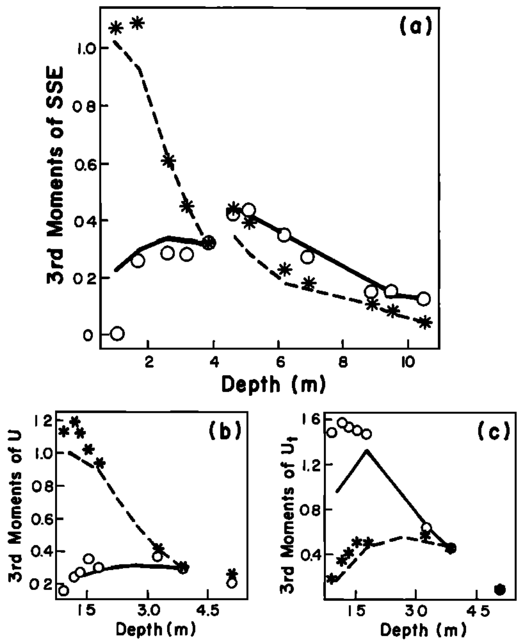

Fig. 4. Predicted and observed normalized third moments versus depth for the narrow-band swell data ($h > 4$ m, Torrey Pines (S11); $h \leq 4$ m, Santa Barbara (F2)): (*a*) sea surface elevation, (*b*) near-bottom horizontal velocity, and (*c*) near-bottom horizontal acceleration. Solid and dashed lines are Boussinesq model predictions of skewness and asymmetry, respectively. Circles and asterisks are observed values of skewness and asymmetry, respectively.

observed values of biphase for the triads shown in Figure 6 and other triads consisting of the primary and/or its higher harmonics are very accurately predicted by the Boussinesq model.

The strength of the nonlinear interactions among the three modes of a particular triad is quantified by the bicoherence and is shown in Figure 6 for the (f_p, f_p, f_{2p}) and (f_p, f_{2p}, f_{3p}) interactions of the swell-dominated data. Even at the seaward edge of the shoaling region, there is some nonlinear coupling between motions at the power spectral peak frequency and those at its first harmonic (see also *Hasselman et al.* [1963]). The coupling increases in strength (i.e., increasing bicoherence) as the waves shoal and is very accurately predicted by the Boussinesq model (Figure 6). As more and more triads become nearly resonant in shallower water and as amplitudes increase during shoaling, both data and model predictions show that nonlinear interactions spread to encompass higher harmonics of the primary peak as well as many other frequencies, including frequencies as low as $f = 0.01$ Hz.

4.2. *Broadband Wave Fields*

A second class of commonly observed wave fields consists of locally generated waves characterized by a relatively broadband power spectrum, as illustrated by F15 in Figure 1. Although the shape of the power spectrum at the seaward edge of the shoaling region differs from the narrow-band wave field discussed above, many aspects of the evolution during shoaling are similar. In particular, the wave shapes undergo similar shoaling evolution from sinusoidal to sawtooth profiles.

As in the narrow-band case, LFDT and the Boussinesq model both predict well the observed evolution of second moments of sea surface elevation, velocity, and acceleration (Figure 7). However, as discussed above, third moments (i.e., wave shape) may be critical for calculating net sediment transport.

For broadband wave fields the total skewness and asymmetry are not dominated by contributions from a few isolated harmonic triads, as was the case with narrow-band wave fields. Rather, nonlinear interactions significantly couple many frequencies within the wind wave band, with each triad of coupled waves contributing to the overall third moments. The biphases of all these triads approach −90° as the waves shoal [*Elgar and Guza*, 1985*b*]. It is well known that the assumptions underlying the Boussinesq model become invalid at high frequencies where kh is large and the lowest-order Boussinesq dispersion relation deviates significantly from the exact finite depth solution. Thus it is not surprising that nonlinear model predictions of third moments for broad-banded conditions (Figure 8) are not as accurate as those for swell-like spectra (Figure 4). This is especially true for acceleration statistics (Figure 8*c*), where high-frequency motions are even more important [*Elgar et al.*, 1988]. Nonetheless, the nonlinear model correctly predicts the depth-dependent trends in the third moments of sea surface elevation, horizontal velocity, and acceleration.

4.3. *Wave Fields With Bimodal Spectra*

A third generic wave field has both low-frequency swell and higher-frequency sea peaks separated by a spectral valley (S16 and F12 in Figure 1). The swell and sea in these data sets arrived at the outer edge of the shoaling region from

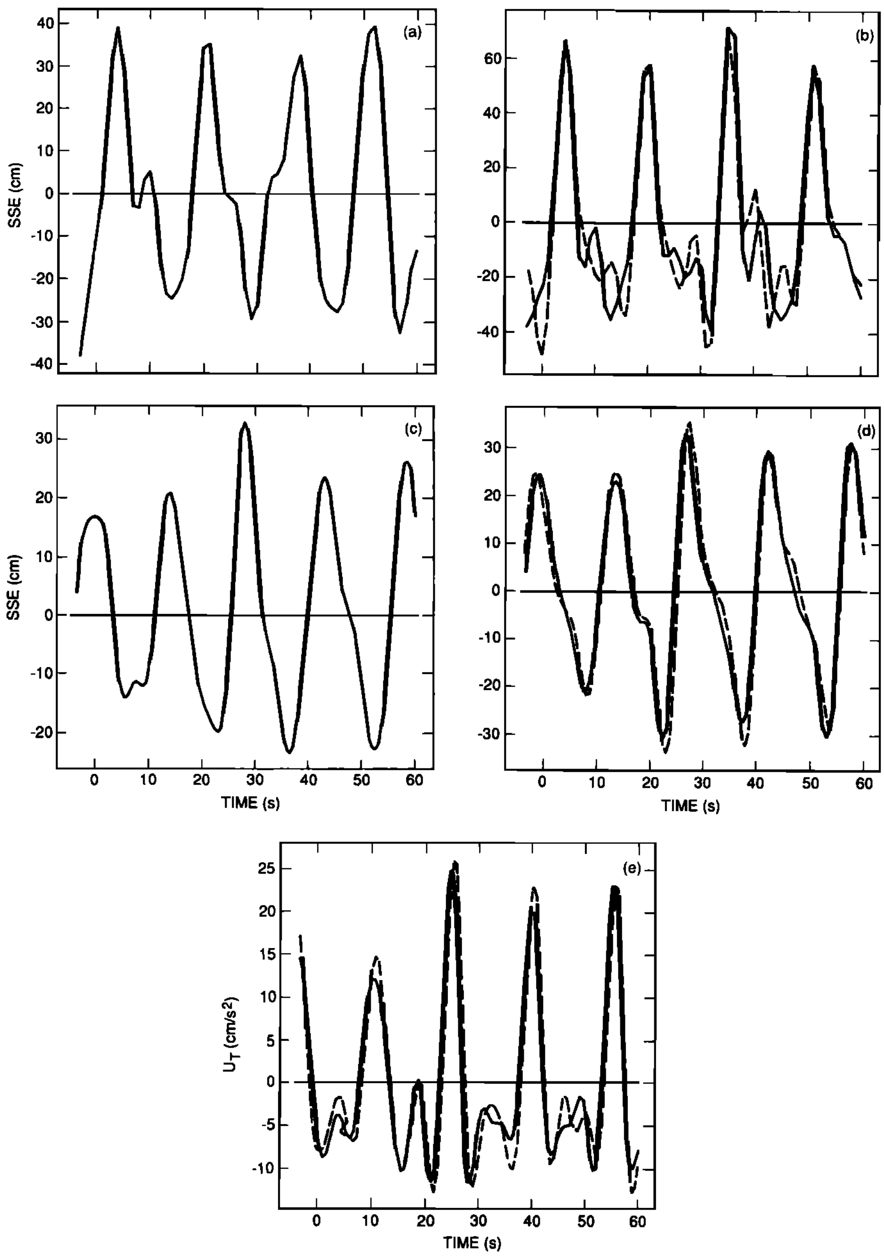

Fig. 5. (*a*–*d*) Sea surface elevation and (*e*) horizontal acceleration versus time. (*a*) Torrey Pines initial conditions (S11), depth of 10 m; (*b*) Torrey Pines (S11), depth of 4.5 m; (*c*) Santa Barbara initial conditions (F2), depth of 4.0 m; (*d*) Santa Barbara (F2), depth of 1.5 m; (*e*) Santa Barbara (F2) horizontal acceleration, depth of 1.5 m. The solid lines are Boussinesq model predictions, and the dashed lines are observations. The data have been band pass filtered between 0.05 and 0.2 Hz in order to isolate the primary and its first two harmonics.

significantly different directions. *Elgar and Guza* [1985*a*] discuss F12, which had a separation of about 45° between the central angles of each power spectral peak. For S16 the sea and swell were separated by about 25°. The evolution of sea surface elevation variance is qualitatively well predicted by both LFDT and the nonlinear model (Figure 9*a*). As in the narrow-band and broad-band cases discussed above, the steepening of the wave profile during shoaling is fairly well predicted by the Boussinesq model, as shown in Figure 10*a*. The predictions of near-bottom velocity variance (Figure 9*b*) and third moments (Figures 10*b* and 10*c*) are considerably less accurate, perhaps owing to directional effects.

Bicoherence spectra indicate that there is nonlinear transfer of energy into frequency bands in the spectral valley ($f \sim$ 0.15 Hz in F12, Figure 1) from sum interactions within the swell peak as well as from difference interactions between the sea and swell [*Elgar and Guza*, 1985*b*]. The biphase of the difference interaction is close to 180° in the seaward portion of the shoaling region and decreases as the waves propagate shoreward (Figure 11). The biphase evolution is well predicted by the nonlinear model, as is the bicoherence of this triad. It is interesting to note that as the spectral valley fills in and the sea peak energy decreases, the strength of the coupling within the triad consisting of swell, sea, and their difference frequency decreases. At the shallowest sensor the power spectrum is relatively flat for frequencies above the swell peak, and bicoherence spectra indicate that there are many interacting triads, similar to the broadband spectrum described above.

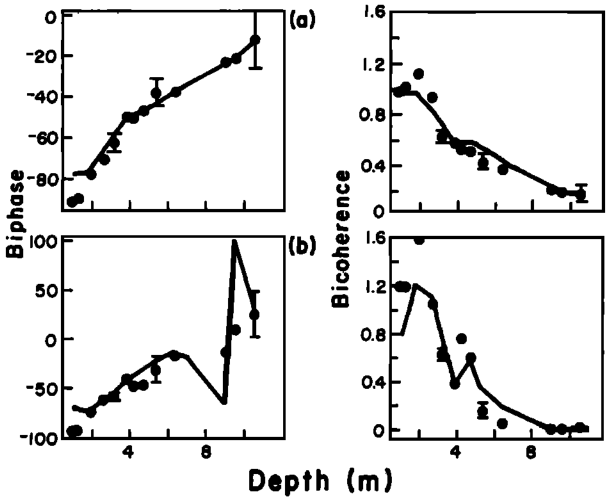

Fig. 6. Biphase (degrees, left panels) and bicoherence (right panels) of sea surface elevation versus depth ($h > 4$ m, Torrey Pines (S11); $h \leq 4$ m, Santa Barbara (F2)): (*a*) the triad consisting of the power spectral primary peak frequency and its first harmonic and (*b*) the triad consisting of the primary, first harmonic, and second harmonic. The solid lines are Boussinesq model predictions, and the solid circles are field observations. The bars are 90% confidence limits [*Elgar and Sebert*, 1989] of the observed quantities.

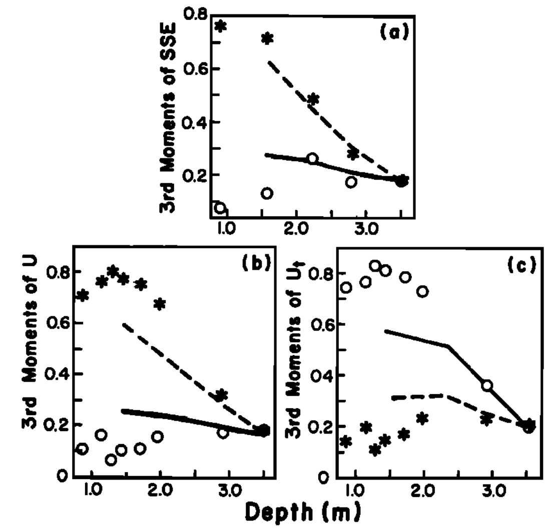

Fig. 8. Predicted and observed normalized third moments versus depth for the broadband data, Santa Barbara (F15): (*a*) sea surface elevation; (*b*) near-bottom horizontal velocity; and (*c*) near-bottom horizontal acceleration. Format is the same as Figure 4.

4.4. *Many Spectral Shapes*

From the selected cases discussed above it is clear that the Boussinesq model at least qualitatively predicts the evolution of second and third moments of shoaling waves for the conditions considered. Model-data comparisons for many more data sets (Table 1) are now summarized.

Predictions of third moments of sea surface elevation and near-bottom horizontal velocity and acceleration are com-

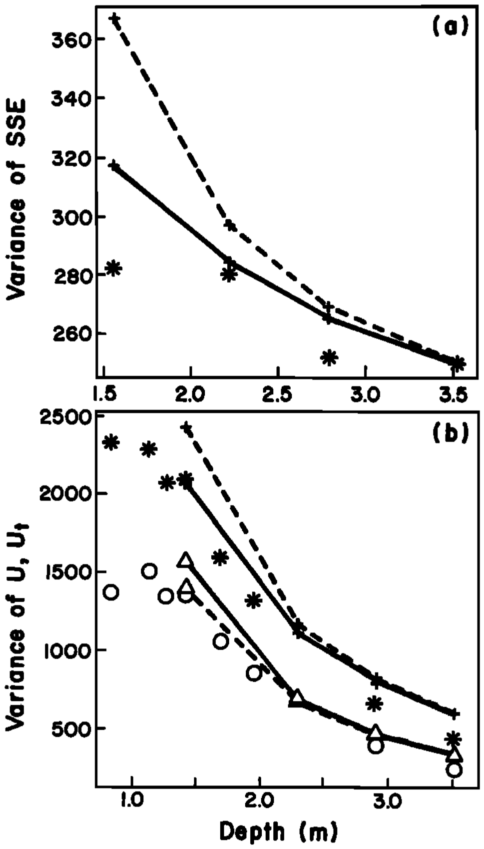

Fig. 7. Predicted and observed second moments versus depth for the broadband Santa Barbara (F15) data: (*a*) sea surface elevation and (*b*) near-bottom horizontal velocity and near-bottom horizontal acceleration. Format is the same as Figure 2.

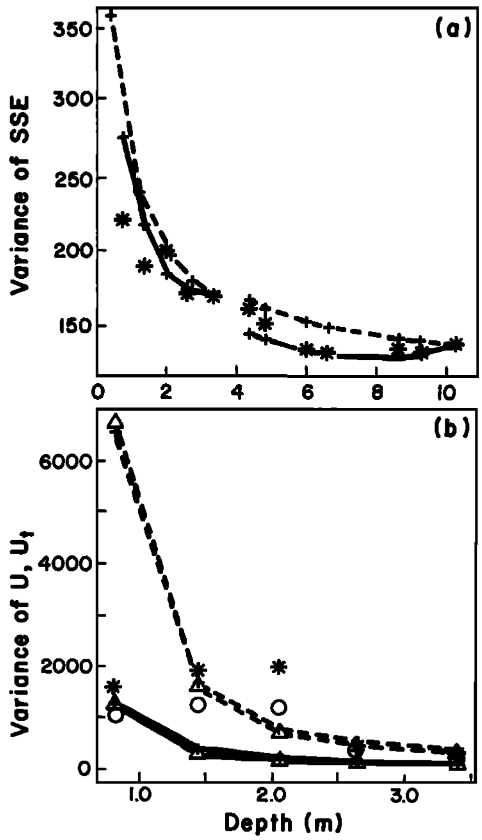

Fig. 9. Predicted and observed second moments versus depth for the bimodal data ($h > 4$ m, Torrey Pines (S16); $h \leq 4$ m, Santa Barbara (F12)): (*a*) sea surface elevation and (*b*) near-bottom horizontal velocity and near-bottom horizontal acceleration. Format is the same as Figure 2.

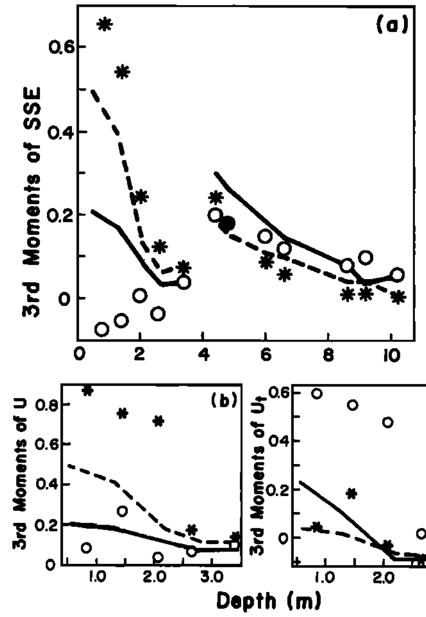

Fig. 10. Predicted and observed normalized third moments versus depth for the bimodal data ($h > 4$ m, Torrey Pines (S16); $h \leq 4$ m, Santa Barbara (F12)): (*a*) sea surface elevation; (*b*) near-bottom horizontal velocity; and (*c*) near-bottom horizontal acceleration. Format is the same as Figure 4.

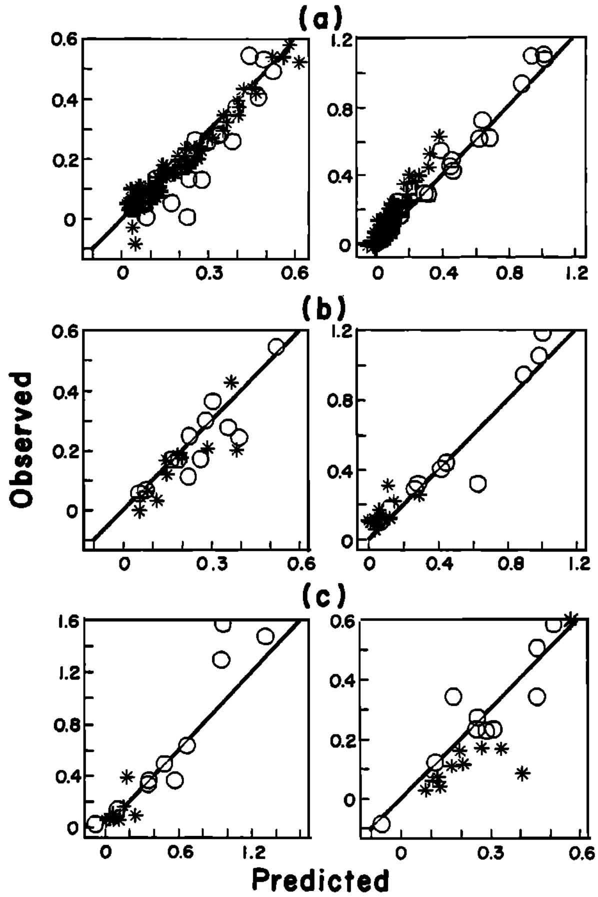

Fig. 12. Observed normalized third moments versus Boussinesq model predictions of normalized third moments of (left) skewness and (right) asymmetry: (*a*) sea surface elevation; (*b*) near-bottom horizontal velocity; (*c*) near-bottom horizontal acceleration. Asterisks are Torrey Pines, and circles are Santa Barbara. Values falling on the 45° solid lines correspond to perfect agreement between data and model predictions.

pared to observed values in Figure 12. The Boussinesq model predictions of sea surface elevation skewness and asymmetry are accurate for both field sites, although the predicted sea surface elevation asymmetry for the Torrey Pines data (Figure 12*a*) is systematically somewhat less than observed values. Model predictions of third moments of near-bottom velocity 250 m from the initial conditions at Torrey Pines ($h \approx 4.5$ m) and 12–56 m from the initial conditions at Santa Barbara are compared to observations in Figure 12*b*. Overall, the predictions are good. The four overpredicted values of Santa Barbara velocity skewness (Figure 12*b*) correspond to the shallowest sensor on each of four days where there was some dissipation of the wave field and where the model is known to overpredict spectral levels at high frequencies. The Boussinesq model predicts acceleration skewness and asymmetry somewhat less accurately (Figure 12*c*).

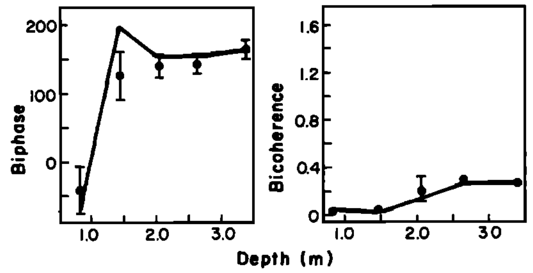

Fig. 11. Biphase (degrees, left panel) and bicoherence (right panel) of sea surface elevation for the triad consisting of waves from the swell and sea peaks, and their difference frequency for F12 versus depth. The solid lines are Boussinesq model predictions, and the solid circles are field observations. The bars are 90% confidence limits [*Elgar and Sebert*, 1989] of the observed quantities.

5. CONCLUSIONS

The evolution of waves through the shoaling region, and in particular third moments of the wave field, is well described by the Boussinesq equations. Given the wave field at the seaward edge of the shoaling region, the wave statistics up to the zone of wave breaking are accurately predicted, as demonstrated by the model-data comparisons presented here. The physics of the Boussinesq model involves nonlinear triad interactions among waves at all frequencies that nearly satisfy the resonance conditions. As the waves shoal, progressively higher frequency motions become involved in nonlinear interactions, and spectral energy transfers and nonlinear phase changes become stronger and spread to encompass waves at nearly all frequencies within the swell and wind wave bands. The Boussinesq model is not limited to any particular spectral shape and accurately predicts the evolution of wave fields composed of swell, locally generated sea, combinations of swell and sea, or other typical field conditions. The nonlinear model is not dependent on the particular field location as long as dissipation is negligible and the bathymetry is suitably smooth. At the two beaches considered here the predictive skill of the model is excellent.

Acknowledgments. Support for this analysis was provided by the Physical Oceanography Program of the National Science Foundation (OCE-8612008) and the Coastal Sciences Branch of the Office of Naval Research. The data collection was supported by ONR (Torrey Pines) and the Sea Grant Nearshore Sediment Transport Study (Santa Barbara). E. B. Thornton, R. L. Lowe, and R. J. Seymour contributed significantly to the field experiments. Portions of the analysis were performed at the Jet Propulsion Laboratory, California Institute of Technology, under contract to NASA. The computations were performed at the San Diego Supercomputer Center (supported by NSF).

REFERENCES

Abbott, M. B., H. M. Peterson, and O. Skovgaard, On the numerical modelling of short waves in shallow water, *J. Hydraul. Res.*, *16*, 173–203, 1978.

Bailard, J. A., and D. L. Inman, An energetics bedload model for a plane sloping beach: Local transport, *J. Geophys. Res.*, *86*, 2035–2043, 1981.

Battjes, J. A., J. P. F. M. Janssen, Energy loss and set-up due to breaking of random waves, in *Proceedings of the 16th International Conference on Coastal Engineering*, pp. 569–576, American Society of Civil Engineers, New York, 1978.

Bjiker, E. W., E. van Hijum, and P. Vallinga, Sand transport by waves, in *Proceedings of the 15th International Conference on Coastal Engineering*, pp. 1149–1166, American Society of Civil Engineers, New York, 1976.

Boczar-Karakiewicz, B., and R. Davidson-Arnott, Nearshore bar formation by nonlinear wave processes-A comparison of model results and field data, *Mar. Geol.*, *77*, 287–304, 1987.

Bowen, A. J., Simple models of nearshore sedimentation; beach profiles and longshore bars, in *The Coastline of Canada*, edited by S. B. McCann, pp. 1–11, Geological Survey of Canada, Ottawa, 1980.

Collins, J. I., Prediction of shallow-water spectra, *J. Geophys. Res.*, *77*, 2693–2707, 1972.

Dally, W. R., R. G. Dean, and R. A. Dalrymple, Wave height variation across beaches of arbitrary profile, *J. Geophys. Res.*, *90*, 11,917–11,927, 1985.

Doering, J. C., and A. J. Bowen, Skewness in the nearshore zone: A comparison of estimates from Marsh-McBirney current meters and colocated pressure sensors, *J. Geophys. Res.*, *92*, 13,173–13,183, 1987.

Elgar, S., Relationships involving third moments and bispectra of a harmonic process, *IEEE Trans. Acoust. Speech Signal Process.*, *12*, 1725–1726, 1987.

Elgar, S., and R. T. Guza, Shoaling gravity waves: Comparisons between field observations, linear theory, and a nonlinear model, *J. Fluid Mech.*, *158*, 47–70, 1985*a*.

Elgar, S., and R. T. Guza, Observations of bispectra of shoaling surface gravity waves, *J. Fluid Mech.*, *161*, 425–448, 1985*b*.

Elgar, S., and R. T. Guza, Nonlinear model predictions of bispectra of shoaling surface gravity waves, *J. Fluid Mech.*, *167*, 1–18, 1986.

Elgar, S., and G. Sebert, Statistics of bicoherence and biphase, *J. Geophys. Res.*, *94*, 10,993–10,998, 1989.

Elgar, S., R. T. Guza, and M. H. Freilich, Eulerian measurements of horizontal accelerations in shoaling gravity waves, *J. Geophys. Res.*, *93*, 9261–9269, 1988.

Elgar, S., M. H. Freilich, and R. T. Guza, Recurrence in truncated Boussinesq models for nonlinear waves in shallow water, *J. Geophys. Res.*, *95*, 11,547–11,556, 1990.

Freilich, M. H., and R. T. Guza, Nonlinear effects on shoaling surface gravity waves, *Philos. Trans. R. Soc. London, Ser. A*, *311*, 1–41, 1984.

Freilich, M. H., R. T. Guza, and S. Elgar, Observations of nonlinear effects in directional spectra of shoaling surface gravity waves, *J. Geophys. Res.*, *95*, 9645–9656, 1990.

Guza, R. T., and E. B. Thornton, Local and shoaled comparisons of sea surface elevations, pressures and velocities, *J. Geophys. Res.*, *85*, 1524–1530, 1980.

Guza, R. T., and E. B. Thornton, Velocity moments in nearshore, *J. Waterw. Port Coastal Ocean Div. Am. Soc. Civ. Eng.*, *111*, 235–256, 1985.

Hanes, D., and D. Huntley, Continuous measurements of suspended sand concentration in a wave dominated nearshore environment, *Cont. Shelf Res.*, *6*, 585–596, 1986.

Hasselman, K., W. Munk, and G. MacDonald, Bispectra of ocean waves, in *Time Series Analysis*, edited by M. Rosenblatt, pp. 125–139, John Wiley, New York, 1963.

Lé Mehauté, B., and J. D. Webb, Wave spectrum changes on a sloped beach, *J. Waterw. Port Coastal Ocean Div. Am. Soc. Civ. Eng.*, *108*, 33–47, 1982.

Liu, P. L.-F, S. B. Yoon, and J. T. Kirby, Nonlinear refraction-diffraction of waves in shallow water, *J. Fluid Mech.*, *153*, 185–201, 1985.

Madsen, P., and I. Warren, Performance of a numerical short-wave model, *Coastal Eng.*, *8*, 73–93, 1984.

Masuda, A., and Y. Kuo, A note on the imaginary part of bispectra, *Deep Sea Res.*, *Part A*, *28*, 213–222, 1981.

Peregrine, D. H., Long waves on a beach, *J. Fluid Mech.*, *27*, 815–827, 1967.

Peregrine, D. H., Equations for water waves and the approximations behind them, in *Waves on Beaches and Resulting Sediment Transport*, edited by R. E. Meyer, pp. 95–122, Academic, San Diego, Calif., 1972.

Peregrine, D. H., Breaking waves on beaches, *Annu. Rev. Fluid Mech.*, *15*, 149–178, 1983.

Rygg, O. B., Nonlinear refraction-diffraction of surface waves in intermediate and shallow water, *Coastal Eng.*, *12*, 191–211, 1988.

Thornton, E. B., and R. T. Guza, Transformations of wave height distribution, *J. Geophys. Res.*, *88*, 5925–5938, 1983.

Thornton, E. B., and R. T. Guza, Surf zone and longshore currents and random waves: Field data and models, *J. Phys. Oceanogr.*, *16*, 1165–1178, 1986.

Yoon, S., and P. Liu, Stem waves along breakwater, *J. Waterw. Port Coastal Harbor Div. Soc. Am. Civ. Eng.*, *115*, 635–648, 1989*a*.

Yoon, S., and P. Liu, Interactions of currents and weakly nonlinear water waves in shallow water, *J. Fluid Mech.*, *205*, 397–419, 1989*b*.

S. Elgar, Electrical and Computer Engineering, Washington State University, Pullman, WA 99164-2752.

M. H. Freilich, Jet Propulsion Laboratory 300-323, 4800 Oak Grove Drive, Pasadena, CA 91109.

R. T. Guza, Center for Coastal Studies, Scripps Institution of Oceanography A-009, La Jolla, CA 92093-0209.

(Received August 2, 1989;
accepted December 20, 1989.)